Electrochimica Acta 145 (2014) 245–253

Contents lists available at ScienceDirect

Electrochimica Acta

journal homepage: www.elsevier.com/locate/electacta

Syntheses and electrochemical properties of the Na-doped $LiNi_{0.5}Mn_{1.5}O_4$ cathode materials for lithium-ion batteries

Jing Wang[a], Weiqing Lin[a], Bihe Wu[a], Jinbao Zhao[a,b,*]

[a] State Key Lab of Physical Chemistry of Solid Surfaces, Department of Chemistry, College of Chemistry and Chemical Engineering, Collaborative Innovation Center of Chemistry for Energy Materials, Xiamen University, Xiamen 361005, P. R, China
[b] School of Energy Research, Xiamen University, Xiamen University, Xiamen 361005, P. R, China

ARTICLE INFO

Article history:
Received 14 May 2014
Received in revised form 24 July 2014
Accepted 25 July 2014
Available online 10 August 2014

Keywords:
$LiNi_{0.5}Mn_{1.5}O_4$
Na-doped
Polarization
Single-crystalline
Lithium ion batteries

ABSTRACT

The novel Na-substituted $Li_{1\text{-}x}Na_xNi_{0.5}Mn_{1.5}O_4$ has been synthesized to use as a cathode material for lithium ion battery via a solid-state method. Both crystal domain size and lattice parameter are influenced by the doping content of Na, without changing the basic spinel structure. The doping of Na ions not only increase the disordered distribution of nickel and manganese cations in spinel, but also increase two additional electron hopping paths, which contribute to a better charge transfer ability, relieve the ohmic polarization and electrochemical polarization of materials and improve lithium ion diffusion coefficient. After Na-doped, the discharge specific capacity rises up comparing to the sample without Na-doped. As a result, the excellent rate capability is achieved for the doping content of 5% Na in spinel, that the discharge capacity is increased by 3.4%, 9.4%, 9.1%, 8.7%, 6.5% and 3.4% in comparison with LNMO, presenting a discharge specific capacity of 121, 119.4, 118.5, 115.1, 108.4 and 101.3mAh·g^{-1} at the rates of 0.2, 0.5, 1, 2, 5 and 10 C respectively, with tiny Mn^{3+} platform appearing. In addition, the sample presents a discharge capacity of 125mAh·g^{-1} at 1 C, with a retention of 116.2mAh g^{-1} after 100 cycles. Even cycling at 5 C rate and 55 °C, the cell with 5% Na-doped LNMO cathode can has 82% of capacity retention after 400 cycles, indicating that it is a promising cathode material for lithium ion batteries.

1. Introduction

Due to high energy, high power density, high working voltage and excellent cyclic performance [1,2], lithium ion battery has become one of the main power supply sources for mobile phones, digital cameras, laptop computers and so on. With the lithium ion battery expansion to electric vehicle (EV), hybrid electric vehicle (HEV), plug-in hybrid electric vehicle (PHEV), communication technology and mobile storage devices field [3], the performance of lithium ion battery, especially the power density and working voltage, is proposed higher and higher requirements to satisfy production and people's demands. Performance of lithium-ion batteries, such as working voltage and power density, is mainly determined by the property of the cathode materials. Therefore, the development of high voltage cathode materials is one important research direction for lithium ion battery with high energy density.

Because of its low cost, little toxicity and good safety performance, spinel $LiMn_2O_4$ (LMO) is thought to be an ideal cathode material for lithium ion batteries [4,5]. Lots of studies have shown that the Fermi energies of the materials are improved and their electrode potentials are raised as a result by doping the spinel $LiMn_2O_4$ materials with a certain amount of transition metal elements M to prepare $LiMn_{2\text{-}x}M_xO_4$ (M = Fe Co Ni Cr etc.) [6]. Of the improved cathode materials with spinel structure, the material $LiNi_{0.5}Mn_{1.5}O_4$ has been shown to have an acceptable performance and stable discharge capacity. It has been reported that there are a high discharge platform existing near 4.7 V and a small platform around 4 V [6,7]. The platform around 4.7 V is assigned to the oxidation-reduction process of Ni^{2+}/Ni^{4+}, while the 4.0 V platform is attributed to the Mn^{3+}/Mn^{4+} oxidation-reduction process. The specific weight energy of the LNMO is greatly improved compared to the conventional cathode materials such as $LiCoO_2$, $LiMn_{1/3}Ni_{1/3}Co_{1/3}O_2$ [8,9], $LiFePO_4$ [10,11] and so on. The LNMO can not only meet the power demands for personal consumer electronics and electric equipment, but also be compatible with high working voltage anode materials such as $Li_4Ti_5O_{12}$ [12,13] and so on. These advances improve the energy density and safety performance of the battery, making it one of the most high-profile positive

---

* Corresponding author at: Corresponding author. Tel.: +86 592 2186935; fax: +86 592 2186935.
E-mail address: jbzhao@xmu.edu.cn (J. Zhao).

http://dx.doi.org/10.1016/j.electacta.2014.07.140
0013-4686/© 2014 Elsevier Ltd. All rights reserved.

electrode material for the next generation advanced lithium ion batteries.

There are two crystallographic structures for LNMO, cation orderly $P4_332$ spinel and disorderly Fd3 m spinel [14,15]. The electrical conductivity of disordered Fd3 m lattice is higher than that of orderly $P4_332$ crystal structure by 2.5 orders of magnitude [14,16]. Because of the disordering character of Ni and Mn, two additional electron hopping paths happen as follows compared with the $P4_332$ dot matrix: $Ni^{2+/3+} \rightarrow Mn^{4+} \rightarrow Ni^{3+/4+}$ and $Ni^{2+/3+} \rightarrow Mn^{4+} \leftrightarrow Mn^{3+} \rightarrow Ni^{3+/4+}$ [17]. The additional electron hopping paths contribute to a better charge transfer ability and relieve the ohmic polarization and electrochemical polarization of materials [18], especially in fast charge-discharge process and at the high temperature state. Studies have found that by doping metal ions such as Ru [19], Cr [20], Co [21], Cu [22], W [23], Nb [24], Mg [25] and so on can increase the disorder extent of nickel and manganese in LNMO, eliminating the formation of the $Li_yNi_{1-y}O$ impurity, thus improve cycling performance of $LiNi_{0.5}Mn_{1.5}O_4$. However, these heavy metal dopants are expensive, limited and environment-unfriendly. In contrast, Na element is cheap, abundant and environmental friendly, which is a promising dopant to substitute for the heavy metals.

In this work, we have successfully synthesized the Na-doped LNMO. The doping of Na element can increase the cation disordered degree of nickel and manganese of LNMO. When the doping amount was 5% ($n_{Na}/n_{(Na + Li)}$, mole ratio), the material presents optimal cycle performance and rate performance.

2. Experimental

2.1. Material preparation

The plate-like $[Mn_{0.75}Ni_{0.25}](OH)_2$ were prepared by a co-precipitation method. An aqueous solution of $NiSO_4 \cdot 6H_2O$ and $MnSO_4 \cdot 5H_2O$ with a concentration of 2.0mol·L^{-1} was pumped into a continuously stirred beaker (1L) under an N_2 atmosphere. At the same time, a mixed solution of NaOH (4.0mol·L^{-1}) and desired amount of NH_4OH solution as a chelating agent were pumped into the reactor. The concentration, pH, temperature and stirring speed of the mixture in the reactor were carefully regulated. The resultant slurry was aged in the beaker under an N_2 atmosphere at 55 °C for 12 h, then the sheet-like hydroxides $[Mn_{0.75}Ni_{0.25}](OH)_2$ were obtained. The $[Mn_{0.75}Ni_{0.25}](OH)_2$ powders were filtered and washed using distillated water and alcohol for several times. After air-drying at 100 °C, the obtained particles were mixed with appropriate LiOH and NaOH crystals by a ball mill (FRITSCH-Pulverisette 14) at a speed of 200 rpm for 1 h. Finally, the formed mixture was sintered in air atmosphere at 800 °C for 20 h to obtain $Li_{1-x}Na_xNi_{0.5}Mn_{1.5}O_4$, then cooled to 600 °C, and maintained for 20 h to compensate oxygen vacancy produced with high-temperature pyrolysis before cooling to room temperature slowly. The LNMO doping with 1% Na, 3% Na, 5% Na and 10% Na (Na/Li + Na, in mole ratio) were denoted as 1% Na-LNMO, 3% Na-LNMO, 5% Na-LNMO and 10% Na-LNMO respectively.

2.2. Material characterization

The XRD patterns were collected on a Rigaku miniflex 600 instrument equipping with Cu Kα radiation operated at 40 kV and 15 mA from 10° to 80° at 1° min^{-1} with a step size of 0.02°. Field emission scanning electron microscopy (SEM, HITACHI S-4800) was used to characterize the morphology of samples, and energy dispersive X-ray spectroscopy (EDS, OXFORD 7593-H) as an accessory of SEM was carried out to analyze the element surface distribution of particles with 20 kV acceleration voltage. Transmission electron microscopy (TEM, JEOL-2100) was further used to observe the morphology and identify the structure of the as-prepared samples. Fourier-transformed infrared spectra (FTIR) were determined by a Nicolet 330 infrared spectrometer in transmittance mode using KBr pellet method over the range of 400-1000 cm^{-1}. Raman spectra (JOBIN Yvon Horiba Raman Spectrometer model HR800) were collected by a 10 mW helium/neon laser at 633 nm excitation.

2.3. Electrochemical measurements

Electrochemical performance was evaluated with CR2016-type coin cells. The working electrode film was obtained by spreading a slurry of 70 wt% active material, 20 wt% acetyleneblack, 10 wt% polyvinylidene difluoride (PVDF) binder dispersed in N-methyl pyrrolidione (NMP) solvent onto an current collector of aluminum foil. After drying in a vacuum oven at 100 °C overnight, the film was punched out into a desired size with a punching machine, then roll-pressed. CR2016-type coin cells were assembled by sandwiching a porous polyethylene separator between the electrode and Li metal foil in a high-purity Ar-filled glove box. The electrolyte was 1 mol·L^{-1} $LiPF_6$ salt dissolved in a mixed solution of ethylene carbonate (EC) and dimethyl carbonate (DMC) with a weight ratio of 1:1.

The cells were galvanostatically charged and discharged on a battery test system (LAND CT-2001A instrument,Wuhan, China or NEWARE BTS type battery charger, Shenzhen, China) between 3.5-4.9 V at room temperature at low rates. When the rates higher than 1 C (including 1 C), a two-step charge process (constant current and constant voltage charge) was employed [26]. It meant that following the constant current charge step, the constant voltage charge process was carried out till the current reduced to one tenth of its initial constant value. The specific capacity was calculated basing on the LNMO mass contained in the cell. The current values at various rates were calculated by the theoretical capacity of LNMO. Take 1 C for an example, the current density value at 1 C was 147mA·g^{-1}. Cyclic voltammogram (CV) measurements were performed on a CHI 660D potentiostat at a scan rate of 0.1 mV s^{-1} during a voltage range from 3.1 to 5.0 V. Electrochemical impedance spectra (EIS) tests proceeded on an electrochemical workstation of Solartron SI 1287 at a frequency range from 0.1 Hz to 100 kHz. All the tests were conducted at 25 °C except high temperature tests.

3. Results and discussion

Fig. 1(a-f) show the SEM images of manganese sources $[Mn_{0.75}Ni_{0.25}](OH)_2$, 1% Na-LNMO, 3% Na-LNMO, 5% Na-LNMO and 10% Na-LNMO, respectively. It is found that the precursor $[Mn_{0.75}Ni_{0.25}](OH)_2$ is of a flake-like shape with an average thickness of 50 nm. After calcination, the Na doped LNMO materials are 100-300 nm polyhedrons with clean and smooth surface facets, which indicate perfect crystal of all the samples. Interestingly, the size of the doped-LNMO particles decreases with the increase of doping Na amount. Since the melting point of NaOH is 318.4 °C, which is much lower than that of the LiOH (471 °C), the co-melting state of the precursor during calcination process is easy attained with the increase amount of NaOH, leading to the size of doped LNMO reduces. EDS area mapping analysis presented in Fig. 2 is carried out to further identify the distribution of Na in the samples (the white dots presented Na element). It is clear that all the Na element distribution in the samples is homogeneous and surface distribution densities of the element Na are improved with the Na dopant amounts increase.

XRD analysis is conducted to examine the crystal changes of the samples with different Na-doped quantity. As shown in Fig. 3, all the samples are of well-defined cubic spinel structure, without the rock salt phase $Li_{1-x}Ni_xO$ which normally emerges at 37.51°,

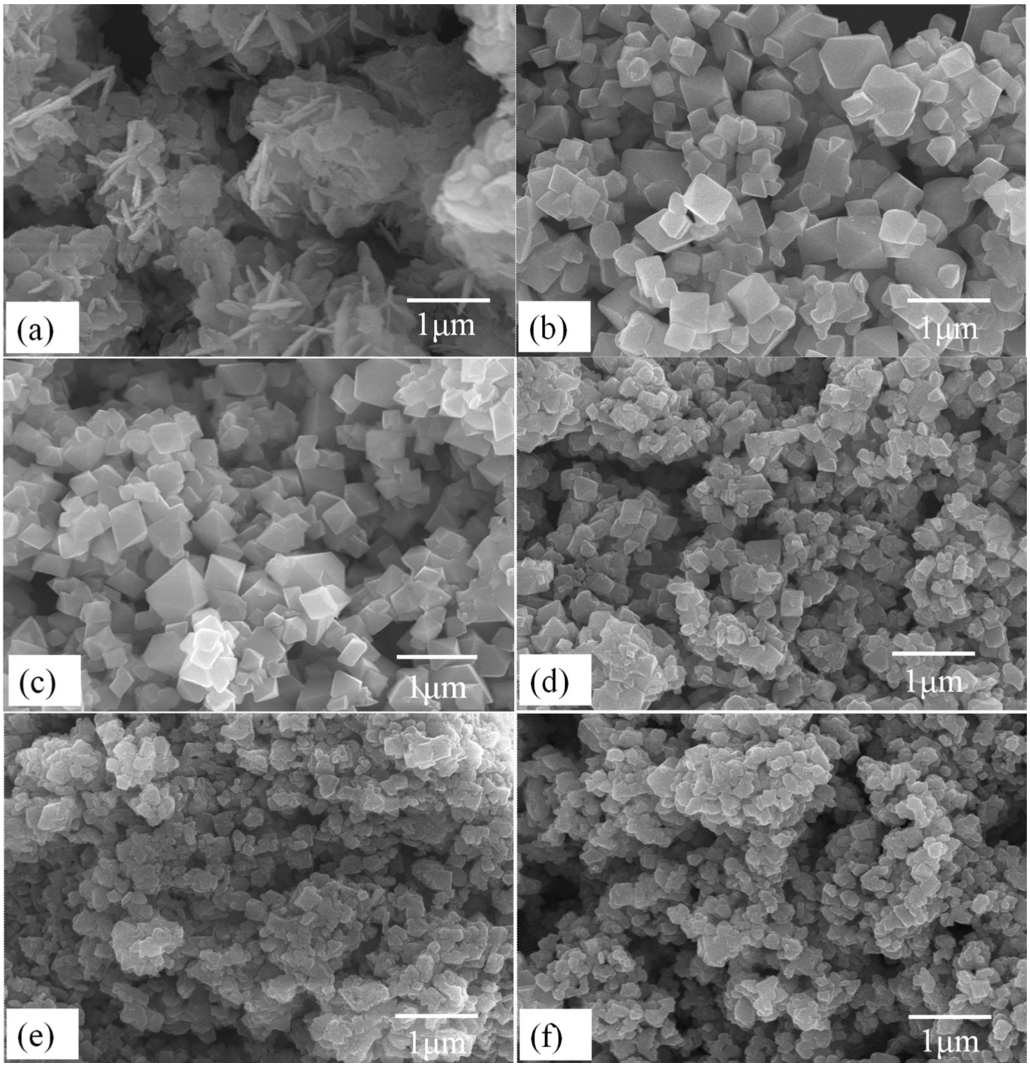

Fig. 1. SEM patterns: (a) $[Mn_{0.75}Ni_{0.25}](OH)_2$, (b)LNMO, (c)1% Na-LNMO, (d)3% Na-LNMO, (e)5% Na-LNMO and (f)10% Na-LNMO.

43.62° and 63.42°. It is reasonable to assume the annealing at 600 °C could compensate the oxygen vacancy produced at high-temperature calcination (above 600 °C). However, when the doping content is up to 10%, there emerge two little peaks. The peak at 12.85° in XRD patterns of the samples is attributed to the $Mn_{0.98}O_2$, while the peak at 15.85° is ascribed to the phase of the $Na_2Mn_3O_7$ due to the addition of the excessive Na element. This similar phenomenon was also reported by Na-doped $Li_4Ti_5O_{12}$ [27]. When a quarter of lithium ions were substituted by sodium ions, denoted as $Li_3NaTi_5O_{12}$, three crystalline phases appeared in the resulting sample: dominant $NaLiTi_3O_7$ phase with an orthorhombic structure (JCPDS 52-0690), a small fraction of $Li_4Ti_5O_{12}$, and a trace of Li_2TiO_3 phase. The Bragg peaks move to low angle after Na-doped as shown in Fig. 3 inset. The lattice parameters, interlayer space of (111) lattice plane and the integrated intensity ratios of the (400)/(311) are obtained from the least square refinement based on a cubic structure by the PDXL2 software (Rigaku, Japan), and the results are summarized in Table 1. As seen from the Table 1, the crystal lattice parameter and interlayer space of (111) lattice plane for the LNMO are 8.131 Å and 4.668 Å. On the base of Xiao's [10] and Yang's [22] reports, the crystal lattice parameter of LNMO is about 8.17 Å, some larger than 8.131 Å of our samples prepared in this paper. It is likely that in our experiment, oxygen vacancy in our samples which were annealed at 600 °C for 20 h becomes less and the amount of Mn^{3+} is also lower than their materials which can be seen from the discharge curve. As a result, the valency of most of Mn ions in the samples is +4. So we think that the shrink of lattice parameter could be ascribed to the smaller ionic radius of Mn^{4+} (0.54 Å) rather than Mn^{3+} (0.645 Å). Together with the Na content increase from 1% to 3% and 5%, the crystal lattice parameters increase gradually from 8.151 Å to 8.159 Å and 8.163 Å, respectively. When the Na content is up to 10%, the crystal lattice parameter reachs up to 8.166 Å. The interlayer space of (111) lattice plane for the Na-doped LNMO shows the same increase trend with the Na content increased to 10%. It is worth noting that the lattice parameters and interlayer space of (111) lattice plane swell slightly after the substitutions, suggesting Na^+ (1.02 Å) with the bigger ionic radius substituting Li^+ (0.76 Å) in the materials occurs. The Na is most likely to substitute Li according to other people's research.

Table 1
The summary of the as-synthesized samples of lattice parameters for all samples (a, b, c, a = b = c), d_{111}, and the integrated intensity ratios of the (400)/(311).

	a(Å)	d_{111} (Å)	I(400)/I(311)
LNMO	8.131	4.668	1.154
1% Na-LNMO	8.151	4.695	1.086
3% Na-LNMO	8.159	4.702	1.062
5% Na-LNMO	8.163	4.706	1.047
10% Na-LNMO	8.166	4.717	1.025

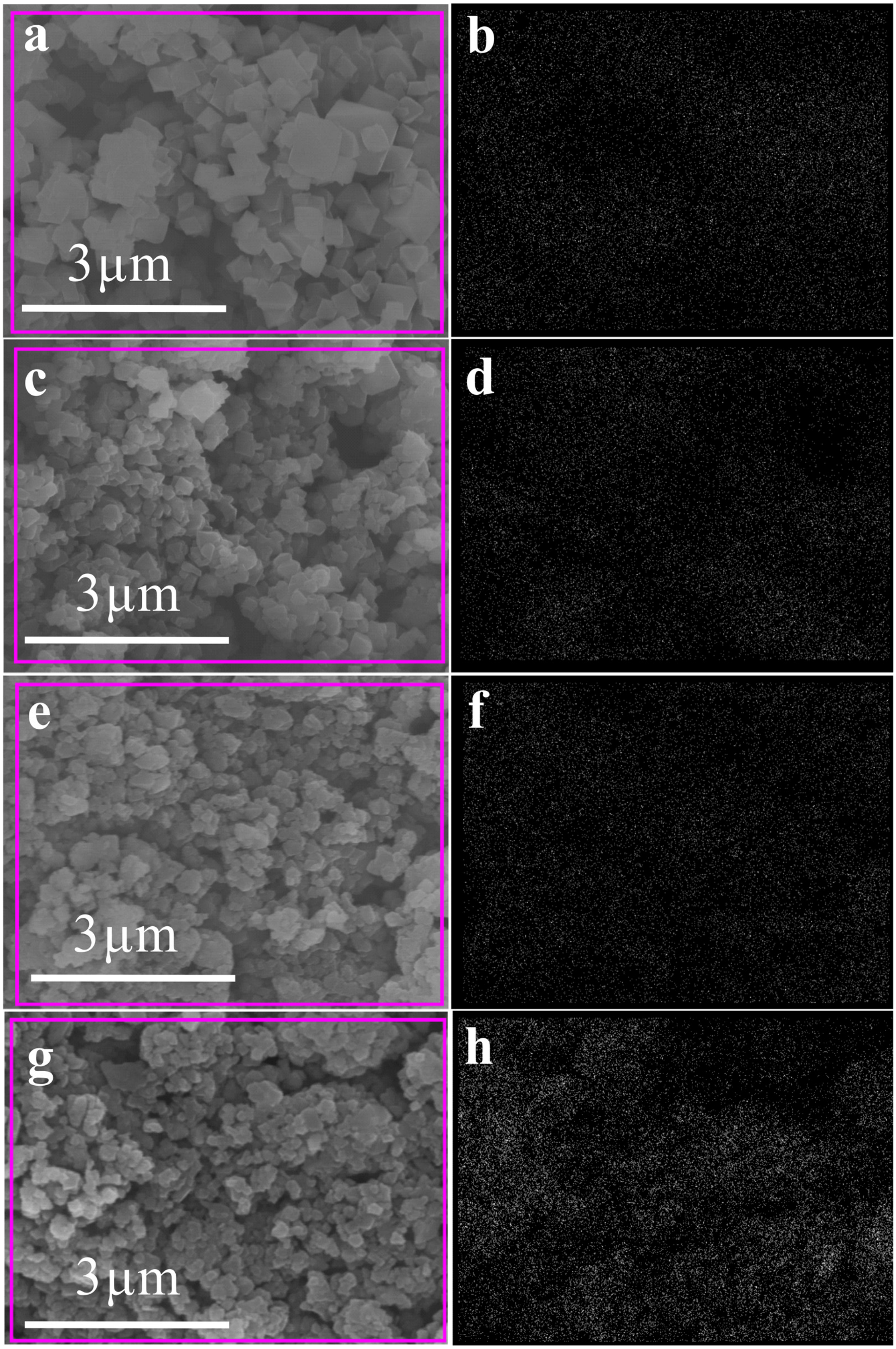

Fig. 2. EDS area mappings of Na element of samples and corresponding region in SEM plots: (a, e) 1%-Na LNMO, (b, f) 3% Na-LNMO, (c, g) 5% Na-LNMO, (d, h) 10% Na-LNMO.

Ellis [28], Xiao [27] and He [29] synthesized A_2MPO_4F Fluorophosphates(A = Na, Li; M = Fe, Mn, Co, Ni), $Li_{4-x}Na_xTi_5O_{12}$ and Na-doped $Li_{1.2}[Co_{0.13}Ni_{0.13}Mn_{0.54}]O_2$ for lithium ion battery, respectively, and they all thought Na occupied Li sites in crystal structure. During the high temperature calcination process, ion-mixed phenomenon may happened, trace amount of Na may entered into the Ni and Mn sites, also the Na^+ (1.02 Å) radius is bigger than Ni^{2+} (0.69 Å) and Mn^{4+} (0.54 Å). Most of Na ions substitute Li in spinel, because the discharge capacity of LNMO increased after moderate Na doping, and trace amount of Na ions which may enter into Ni and Mn sites will not extract from the spinel. According to Ohzuku et al. [30], the extent of occupancy of the substituent ions in the 8a lithium sites is presented by the integrated intensity ratios of the (400)/(311) peaks. The intensity ratio of the (400)/(311) peaks for the LNMO is

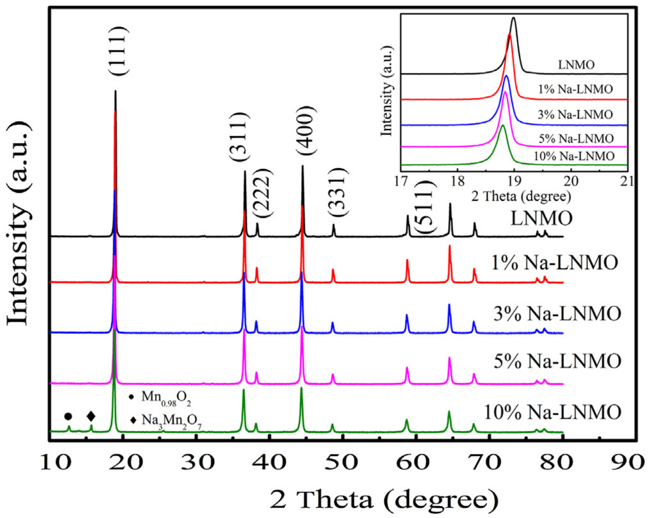

Fig. 3. XRD patterns of samples.

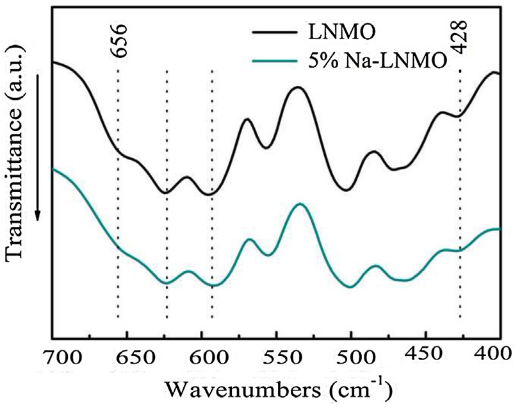

Fig. 4. FT-IR spectra of LNMO and 5% Na-LNMO.

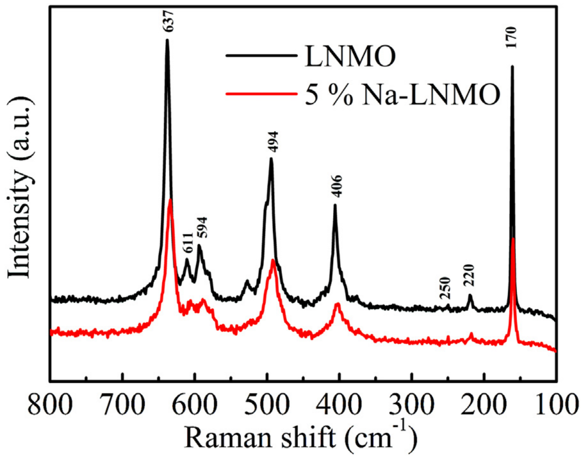

Fig. 5. Raman spectra of LNMO and 5% Na-LNMO.

1.154 and reduces with the increase of Na content, suggesting that more Na occupy the 8a lithium sites in the LNMO, which is consistent with our assumption that Na enter into Li sites. There are not any visible differences between the $P4_332$ and Fd3 m spinel in the XRD characterization.

IR spectroscopy, an effective technique in identification of the $P4_332$ and Fd3 m spinel of the LNMO [31], is further applied to characterize the structure of Na-doped LNMO. According to Patoux [32], in general synthesis, the LNMO is usually a mixture of ordered $P4_332$ phase and disordered Fd3 m phase. As shown in Fig. 4, the bands at 428 and 656 cm^{-1} which are the characteristic peaks of the $P4_332$ spinel [33] turn to be weakened after 5% Na doped, indicating that the Na-doping destroyed the ordering of Ni and Mn ions, so the proportion of Fd3 m spinel increase with the rise of Na content. The difference between LNMO and 5% Na-LNMO was further examined by Raman spectroscopy, as shown in Fig. 5. According to previously report [34,35], the strong band appeared at 637 cm^{-1} is attributed to the symmetrical Mn-O stretching vibration (A_{1g}) in MnO_6 octahedra. Peaks around 406 and 494 are related to the Ni^{2+}-O stretching mode in spinel. $T_{2g}{}^{(3)}$ of the spinel is present at around 590-615 cm^{-1}. The split of this $T_{2g}{}^{(3)}$ band is the fingerprint of $P4_332$ space group. In Fig. 5, the splitting of $T_{2g}{}^{(3)}$, a doublet at 594 and 611 cm^{-1}, can be clearly observed for LNMO. The other characteristic peaks of $P4_332$ structure are around 250, 220 and 170 cm^{-1}, which are all present in LNMO spectra [31,36]. For the 5% Na-LNMO, all of these peaks are weaken, especially characteristic peak at 611 cm^{-1}, indicating that the percentage of $P4_332$ spinel becomes lower. All this Raman results are consistent with the ones from IR. This may be attributed to the Na-doped improvement of the asymmetry of spinel and to making Ni and Mn more disorderly.

In order to better understand the electrochemical behavior of the samples without and with Na-doped, the CV tests are conducted at the rate of 0.1 mV s^{-1} at 25 °C, and the results are depicted in Fig. 6. Both the intense and sharp reduction/oxidation peaks of Ni^{2+}/Ni^{4+} are observed at around 4.7 V in LNMO and 5% Na-doped LNMO, with trace amount of the couple of Mn^{4+}/Mn^{3+} that usually appears at around 4.0 V shown in inset. After the first activation, the LNMO material exhibits two redox couples at two redox couples at 4.78 V/4.64 V and 4.82 V/4.69 V in CVs plots (Fig. 6) at the sixth cycle, which are attributed to Ni^{3+}/Ni^{2+} and Ni^{4+}/Ni^{3+}, respectively. That two adjacent redox couples for the 5% Na-LNMO are at 4.78 V/4.67 V and 4.80 V/4.70 V with less gap between corresponding oxidation and reduction peak than LNMO, respectively, and their splitting degree and sharp level appear more obviously than that of LNMO, meaning 5% Na-LNMO has the excellent electrochemical reversibility and faster lithium insertion/extraction kinetics [37].

The tenth discharge curve at 1 C discharge rate and the consecutive discharge profiles at 1 C and 25 °C are given in Fig. 7. The tenth discharge capacities of LNMO, 1% Na-LNMO, 3% Na-LNMO, 5% Na-LNMO and 10% Na-LNMO are 112.7, 114.8, 125.3, 123.7 and 106.8mAh·g^{-1}, respectively. After 100 cycles, the specific capacities are 106.1, 106.5, 116.2, 115.6 and 93.9mAh·g^{-1}, respectively. With the Na-doping, the discharge capacities of the LNMO enhance, especially for the 3% Na-LNMO and 5% Na-LNMO. When the doping content is up to 10%, the discharge specific capacity rises down instead. The decrease in capacity may be caused possibly by the existence of large weight ratio of doping agent Na and the impurity formation of $Mn_{0.98}O_2$ and $Na_3Mn_2O_7$. The latter is adverse for electrochemical properties of LNMO. The tenth discharge curve is given in Fig. 7(a), showing that all the discharge curves exhibit two little different potential plateaus around 4.7 V. The results reveal that the Na-doping could not change the basic spinel structure of LNMO, which is consistent with the above XRD results. The platform of the 5% Na-LNMO is the longest among all the samples, which displays the biggest specific capacity.

The first charge and discharge curve of samples at 0.2 C at 25 °C are shown in Fig. 8(a) and (b), respectively. The over-charge phenomena of Na-doped LNMO are more serious than that of LNMO. This is quite likely that Na^+ is more difficult to extracted in the first charge process because of its larger radius, which may generate a bigger overpotential and higher charge voltage [38]. Ellis *et al.* synthesized A_2MPO_4F fluorophosphates (A = Na, Li; M = Fe, Mn, Co, Ni), and found both Li^+ and Na^+ are extracted in the first charge

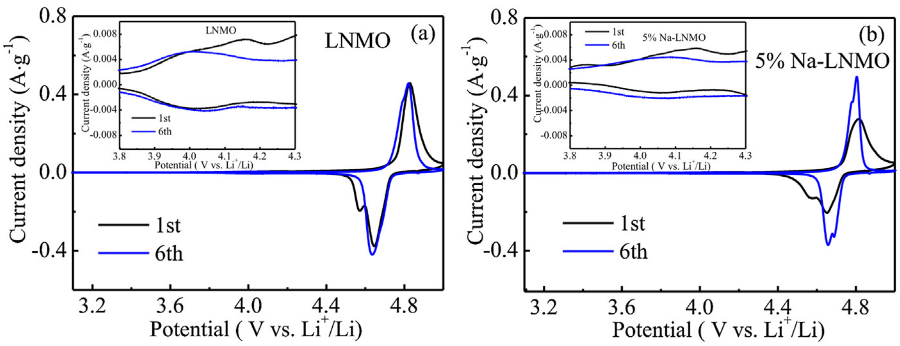

Fig. 6. CVs plots at 25 °C: (a) LNMO, (b) 5% Na-LNMO.

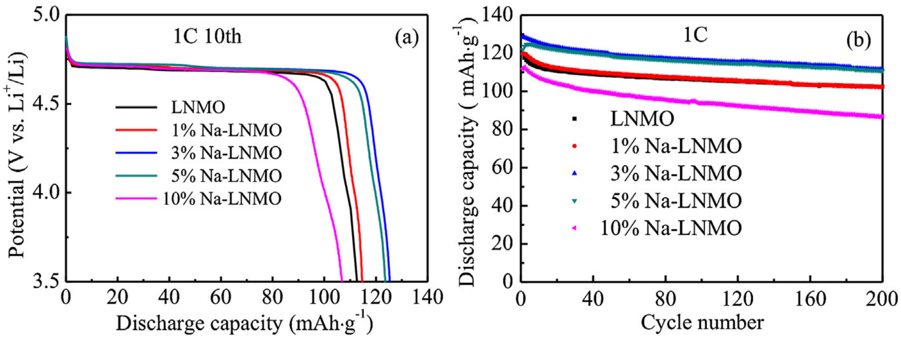

Fig. 7. Electrochemical properties of the as prepared samples: (a) the 10th discharge curve at 1 C; (b) cycle performance at 1 C;.

process, but during the following cycles, only Li^+ ions are possibly inserted/extracted gradually. They think that Li^+ replaces Na^+ in the crystal structure after the first discharging process [28]. The phenomena are also reported by Wu's [38] and Xiao's [27] researches in $Na_2Fe_{1-x}Mn_xPO_4F/C$ and $Li_{4-x}Na_xTi_5O_{12}$ for lithium ion batteries, respectively. So, Na^+ ions in Na-doped LNMO may be extracted during the first charge process, and would not be inserted/removed during the following cycling. As shown in Fig. 8(b), all the samples reveal two major little different discharge platforms at about 4.71 V and 4.67 V, with tiny Mn^{3+} platform around 4.1 V. To investigate the discharge rate capability, the cells are discharged at various constantly mounting discharge rates ranging from 0.2 C to 10 C and then return to 0.5 C and 0.2 C, each sustained for 6 cycles. As shown in Fig. 8(c), after Na-doping, the rate capability of all samples gets

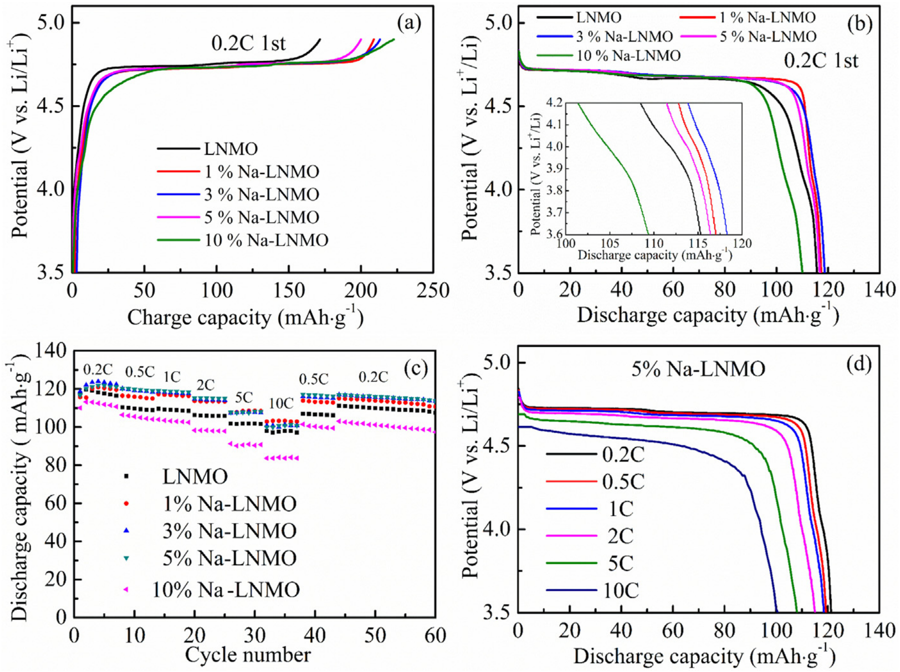

Fig. 8. (a) the first charge curve at 0.2 C at 25 °C, (b) the first discharge curve at 0.2 C at 25 °C (c) rate cycling performance of the samples at 25 °C; (d) discharge profiles of 5% Na-LNMO at different rates at 25 °C.

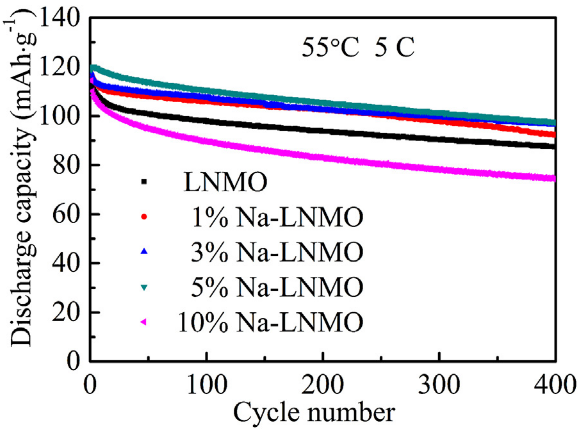

Fig. 9. Cycle performance at 5 C and 55 °C.

a significant enhancement, except for the 10% Na-LNMO, in which structure underwent some changes due to that the impurities in the spinel structure. Of all the synthetic Na-doped LMNO materials, the rate capability of 5% Na-LNMO is the best, exhibiting the discharge capacity of 121, 119.4, 118.5, 115.1, 108.4 and 101.3mAh·g^{-1} at 0.2 C, 0.5 C, 1 C, 2 C, 5 C and10 C respectively, while for the pristine LNMO, the discharge capacities are 117, 109.1, 108.6, 105.9, 101.8 and 98mAh·g^{-1} at the same conditions. As a result of Na-doping, the confusion degree of Ni and Mn increased, so the proportion of the disorderly Fd3 m lattice structure would become higher, with two additional electron hopping paths happened, resulting in less ohmic polarization and electrochemical polarization [18]. In addition, Na-doping improves the interlayer spacing as shown in XRD result, and then increases the lithium ion diffusion coefficient comparing with LNMO. When the discharge current fell from higher rate to 0.2 C after 42 cycles of successive charge-discharge rate variation, the discharge capacity of the 5% Na-LNMO and pristine LNMO maintain at 116 and 109.9mAh·g^{-1}, suggesting that the 5% Na-LNMO are more prominent to have stable structure compared to the pristine LNMO. Fig. 8(d) presents the discharge voltage profiles of the 5% Na-LNMO electrodes at the current rates of 0.2–10 C over a potential window of 4.9–3.5 V. At the initial lower rate of 0.2 C, the 5% Na LNMO electrode show two major discharge platforms at 4.73 V and 4.70 V, respectively. As the discharge current rates increase, the two major voltage platforms decline because of the further electrochemical polarization and ohmic polarization at large current rates. When the current is raised up to 10 C, the discharge voltage plateau is down to 4.5 V without obvious split occurring.

Fig. 9 showed typical cycle performance of the electrodes samples at 5 C rate between 3.5 and 5.0 V at 55 °C. The specific capacity of the LNMO, the 1% Na-LNMO, the 3% Na-LNMO, the 5% Na-LNMO and the 10% Na-LNMO at fifth cycle are 109.5, 113.3, 113.6, 119.7 and 106.7 mAh·g^{-1}, with a retention of 87.6, 92.3, 96.7, 97.6 and 74.6mAh·g^{-1} after 400 cycles, respectively.

Electrochemical impedance spectroscopy (EIS) is carried out to further illustrate the difference in electrochemical polarization and ohmic polarization. All the samples are charged at 1 C by constant current and constant potential process, and discharged via constant current process. Their EIS are measured in the range from 100 kHz to 0.1 Hz after 10 cycles. The Nyquist plots (Fig. 10) of materials display the same profile, a semicircle in the high-frequency region and a linear slop in the low-frequency region, and the equivalent circuits are the same as insets shown. In the equivalent circuit, the Rs is assigned to electrolyte resistance, while the Rct is attributed to direct charge transfer resistance of electrode materials. CPE represents the double layer capacitance and passivation film capacitance. W represents the Warburg impedance. The charge transfer resistances at the interface of electrolyte and electrodes (Rct) for the LNMO, the 1% Na-LNMO, the 3% Na-LNMO, the 5% Na-LNMO and the 10% Na-LNMO are 232, 187.1, 178.5, 108.7 and 144.7 Ω, respectively. The Rct values decrease along with the Na content in spinel except 10% Na-LNMO. The Rct value of 10% Na-LNMO is bigger than that of 5% Na-LNMO, which could be attributed to the existence of $Mn_{0.98}O_2$ and $Na_3Mn_2O_7$. Clearly, the 5% Na-LNMO reveals the smallest charge transfer resistance, which is possibly attributed to the increased confusion level of Ni and Mn ion in the LNMO by Na-doping and higher lithium ion diffusion coefficient. In this case, two additional electron hopping paths happen, which contributes to a better charge transfer ability and electrical conductivity, then relieve the ohmic polarization and electrochemical polarization in a result [18]. The Rct is related to electric conductivity and ion diffusion coefficient, so 10% Na-LNMO had a smaller Rct than LNMO, while low capacity of 10% Na-LNMO is a result of impurity phase of $Mn_{0.98}O_2$ and $Na_2Mn_3O_7$.

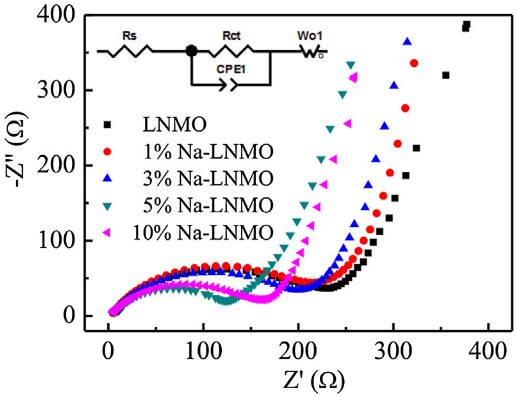

Fig. 10. EIS spectra of the samples in the frequency range between 0.1 Hz and 100k Hz at 25 °C.

In order to further explain the effect of Na doping, the diffusion coefficient of lithium ion can be calculated from the EIS plots (Fig. 10) in the low-frequency region. [2,24] The calculation equation for the D_{Li} values can be denoted as:

$$Z' = Rs + Rct + \sigma\omega^{-0.5} \tag{1}$$

$$D_{Li} = R^2T^2/2A^2n^4F^4C^2\sigma^2 \tag{2}$$

where T, R, A, n, F, C_{Li} and ω are the absolute temperature, the gas constant, the surface area, the number of electrons per molecule during redox process, the Faraday's constant, the concentration of lithium ion, and the angular frequency, respectively. σ is the Warburg factor which is relationship with Z'.

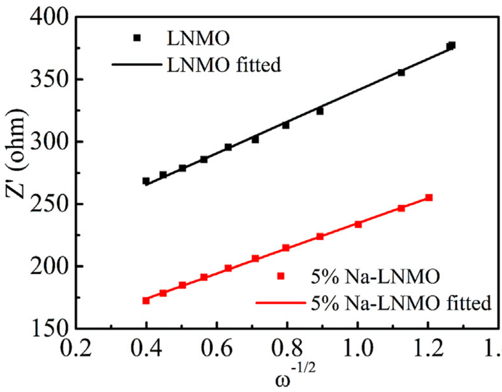

Fig. 11. Z′-ω$^{-0.5}$ pattern in the low-frequency region obtained from EIS measurements of LNMO and 5% Na-LNMO.

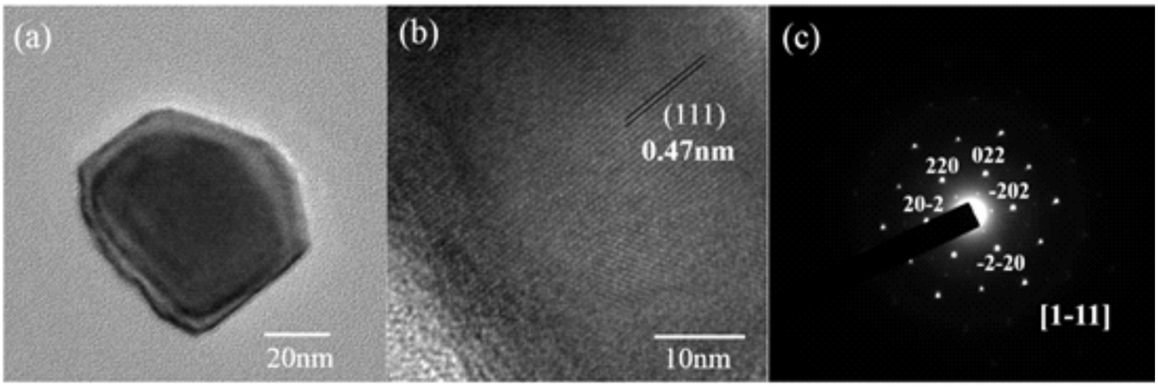

Fig. 12. The as-prepared 5% Na-LNMO of (a) TEM plot, (b) HRTEM image and (c) SAED pattern in the [1–11] zone.

Fig. 11 presents the Z'-$\omega^{-0.5}$ plots, the relationship between the Z' and $\omega^{-0.5}$ acquired from the EIS plots (Fig. 10) in the low-frequency region is linear. According to Eqs. (1) and (2), the lithium ion diffusion coefficients of LNMO and 5% Na-LNMO are calculated to be approximate 1.18×10^{-10} and 1.84×10^{-10} $cm^2 \cdot s^{-1}$, respectively. Obviously, the diffusion coefficient of Li ion is greatly improved due to the Na-doped. This suggests that the increscent interplanar spacing and ion chaotic degree of Ni and Mn are favorable for Li ion migration.

The TEM characterization of the 5% Na-LNMO is displayed in Fig. 12. As shown in Fig. 12(a), the 5% Na-LNMO is of irregular nano-particles. SAED pattern (Fig. 12c) referred to a flat-lying 5% Na-LNMO nano-particle in Fig. 12(a) shows regular hexagonal array of diffraction spots, which is corresponding to the basal plane of its structure, with the electron beam in the [1–11] direction. This regular diffraction spots suggest the as-synthesized 5% Na-LNMO sample are of ordered lattice and single-crystal structure. Fig. 12(b) is a high-resolution TEM (HRTEM) image of this Na-doped $LiNi_{0.5}Mn_{1.5}O_4$ particle, which shows clear lattice fringes. The interplanar spacing lattice in Fig. 12(b) is 0.47 nm, which is in accordance with the d-spacing of the (111) crystal planes of the $LiNi_{0.5}Mn_{1.5}O_4$ [39]. The ordered lattices in long-range order result in the intercalation and deintercalation of Li ion easily occurring, thus enhanced the rate property of the Na-doped LNMO, which is consistent with the electrochemical performance as discussed above.

4. Conclusions

In summary, the Na-doped LNMO are synthesized via a solid-state method. The obtained materials are of good single-crystal with a particle size of approximately 100-300 nm. The doping of Na ions increases the disorder degree of nickel and manganese ion in the spinel structure and improves lithium ion diffusion coefficient, and two additional electron hopping paths happened, which contribute to a better charge transfer ability and resultantly relieve the ohmic polarization and electrochemical polarization of the materials. The doping content of Na up to 5% in the spinel structure exhibited the excellent electrochemical cycle, presenting a discharge specific capacity of $125 mAh \cdot g^{-1}$ at 1 C with a retention of $116.2 mAh \cdot g^{-1}$ after 100 cycles. In addition, it also shows remarkable rate capability, the discharge specific capacity decreased slightly from 121 to 119.4, 118.5, 115.1, 108.4 and $101.3 mAh \cdot g^{-1}$ at 0.2 C, 0.5 C, 1 C, 2 C, 5 C and 10 C, respectively. Furthermore, it has striking electrochemical property at elevated temperature and great rates. At 5 C rate at 55 °C, the discharge capacity of 5% Na-LNMO is up to 119.7 $mAh \cdot g^{-1}$, with a retention of $97.6 mAh \cdot g^{-1}$ after 400 cycles. The high capacity, excellent rate capability, remarkable cycling stability and striking property at elevated temperature of the Na-doped LNMO are obtained, making it a promising cathode material for lithium ion batteries.

Acknowledgements

The authors gratefully acknowledge the financial supports from the National High Technology Research and Development Program of China (2012AA110204) and Key Project of Science and Technology of Xiamen (2013H6022). Weiqing Lin expresses his special thanks to National Found for Fostering Talents of Basic Science (J1310024). The authors also wish to express their thanks to Drs. Peng Zhang, Bo Liu, Jing Yang and Binbin Xu of Xiamen University for their valuable suggestions.

References

[1] D. Liu, J. Trottier, P. Charest, J. Fréchette, A. Guerfi, A. Mauger, C.M. Julien, K. Zaghib, Effect of nano $LiFePO_4$ coating on $LiMn_{1.5}Ni_{0.5}O_4$ 5 V cathode for lithium ion batteries, J. Power Sources 204 (2012) 127–132.
[2] X. Li, W. Guo, Y. Liu, W. He, Z. Xiao, Spinel, $LiNi_{0.5}Mn_{1.5}O_4$ as superior electrode materials for lithium-ion batteries: Ionic liquid assisted synthesis and the effect of CuO coating, Electrochim. Acta 116 (2014) 278–283.
[3] B. Hai, A.K. Shukla, H. Duncan, G. Chen, The effect of particle surface facets on the kinetic properties of $LiMn_{1.5}Ni_{0.5}O_4$ cathode materials, J. Mater. Chem. A 1 (2013) 759–769.
[4] Y.L. Ding, J. Xie, G.S. Cao, T.J. Zhu, H.M. Yu, X.B. Zhao, Single-Crystalline $LiMn_2O_4$ Nanotubes Synthesized Via Template-Engaged Reaction as Cathodes for High-Power Lithium Ion Batteries, Adv. Funct. Mater. 21 (2011) 348–355.
[5] D. Zhan, F. Yang, Q. Zhang, X. Hu, T. Peng, Effect of solid-state reaction temperature on electrochemical performance of $LiMn_2O_4$ submicro-rods as cathode material for Li-ion battery by using γ-MnOOH submicro-rods as self-template, Electrochim. Acta 129 (2014) 364–372.
[6] Y. Wang, G. Yang, Z. Yang, L. Zhang, M. Fu, H. Long, Z. Li, Y. Huang, P. Lu, High power and capacity of $LiNi_{0.5}Mn_{1.5}O_4$ thin films cathodes prepared by pulsed laser deposition, Electrochim. Acta 102 (2013) 416–422.
[7] G.Q. Liu, L. Wen, Y.M. Liu, Spinel, $LiNi_{0.5}Mn_{1.5}O_4$ and its derivatives as cathodes for high-voltage Li-ion batteries, J. Solid State Electrochem. 14 (2010) 2191–2202.
[8] Z. Chang, Z. Chen, F. Wu, H. Tang, Z. Zhu, X.Z. Yuan, H. Wang, Synthesis and characterization of high-density non-spherical $Li(Ni_{1/3}Co_{1/3}Mn_{1/3})O_2$ cathode material for lithium ion batteries by two-step drying method, Electrochim. Acta 53 (2008) 5927–5933.
[9] K. Prasanna, T. Subburaj, Y.N. Jo, C.W. Lee, Optimization of electrophoretic suspension to fabricate $Li[Ni_{1/3}Co_{1/3}Mn_{1/3}]O_2$ based positive electrode for Li-ion batteries, Electrochim. Acta 95 (2013) 295–300.
[10] J. Xiao, X. Chen, P.V. Sushko, M.L. Sushko, L. Kovarik, J. Feng, Z. Deng, J. Zheng, G.L. Graff, Z. Nie, D. Choi, J. Liu, J.G. Zhang, M.S. Whittingham, High-Performance $LiNi_{0.5}Mn_{1.5}O_4$ Spinel Controlled by Mn^{3+} Concentration and Site Disorder, Adv. Mater. 24 (2012) 2109–2116.
[11] J. Du, L.B. Kong, H. Liu, J.B. Liu, M.C. Liu, P. Zhang, Y.C. Luo, L. Kang, Template-free synthesis of porous–$LiFePO_4$/C nanocomposite for high power lithium-ion batteries, Electrochim. Acta 123 (2014) 1–6.
[12] H.G. Jung, M.W. Jang, J. Hassoun, Y.K. Sun, B. Scrosati, A high-rate long-life $Li_4Ti_5O_{12}/Li[Ni_{0.45}Co_{0.1}Mn_{1.45}]O_4$ lithium-ion battery, Nat. Commun. 2 (2011) 516.

[13] X. Li, H. Lin, W. Cui, Q. Xiao, J. Zhao, A Fast Solution-Combustion Synthesis of Nitrogen-Modified $Li_4Ti_5O_{12}$ Nanomaterials with Improved Electrochemical Performance, ACS Appl. Mat. Interfaces (2014).

[14] M. Kunduraci, J.F. Al-Sharab, G.G. Amatucci, High-Power Nanostructured $LiMn_{2-x}Ni_xO_4$ High-Voltage Lithium-Ion Battery Electrode Materials: Electrochemical Impact of Electronic Conductivity and Morphology, Chem. Mater. 18 (2006) 3585–3592.

[15] X. Zhu, X. Li, Y. Zhu, S. Jin, Y. Wang, Y. Qian, $LiNi_{0.5}Mn_{1.5}O_4$ nanostructures with two-phase intergrowth as enhanced cathodes for lithium-ion batteries, Electrochim. Acta 121 (2014) 253–257.

[16] T.F. Yi, Y. Xie, M.F. Ye, L.J. Jiang, R.S. Zhu, Y.R. Zhu, Recent developments in the doping of $LiNi_{0.5}Mn_{1.5}O_4$ cathode material for 5 V lithium-ion batteries, Ionics 17 (2011) 383–389.

[17] Y.C. Jin, C.Y. Lin, J.G. Duh, Improving rate capability of high potential $LiNi_{0.5}Mn_{1.5}O_{4-x}$ cathode materials via increasing oxygen non-stoichiometries, Electrochim. Acta 69 (2012) 45–50.

[18] O. Sha, Z. Tang, S. Wang, W. Yuan, Z. Qiao, Q. Xu, L. Ma, The multi-substituted $LiNi_{0.475}Al_{0.01}Cr_{0.04}Mn_{1.475}O_{3.95}F_{0.05}$ cathode material with excellent rate capability and cycle life, Electrochim. Acta 77 (2012) 250–255.

[19] H. Wang, H. Xia, M.O. Lai, L. Lu, Enhancements of rate capability and cyclic performance of spinel $LiNi_{0.5}Mn_{1.5}O_4$ by trace Ru-doping, Electrochem. Commun. 11 (2009) 1539–1542.

[20] T.F. Yi, J. Shu, Y.R. Zhu, R.S. Zhu, Advanced electrochemical performance of $LiMn_{1.4}Cr_{0.2}Ni_{0.4}O_4$ as 5 V cathode material by citric-acid-assisted method, J. Phys. Chem. Sol. 70 (2009) 153–158.

[21] J. Hassoun, K.S. Lee, Y.K. Sun, B. Scrosati, An Advanced Lithium Ion Battery Based on High Performance Electrode Materials, J. Am. Chem. Soc. 133 (2011) 3139–3143.

[22] M.C. Yang, B. Xu, J.H. Cheng, C.J. Pan, B.J. Hwang, Y.S. Meng, Electronic Structural and Electrochemical Properties of $LiNi_xCu_yMn_{2-x-y}O_4$ ($0 < x < 0.5$, $0 < y < 0.5$) High-Voltage Spinel Materials, Chem. Mater. 23 (2011) 2832–2841.

[23] S.J.R. Prabakar, S.C. Han, S.P. Singh, D.K. Lee, K.S. Sohn, M. Pyo, W-doped $LiW_xNi_{0.5}Mn_{1.5-x}O_4$ cathodes for the improvement of high rate performances in Li ion batteries, J Power Sources 209 (2012) 57–64.

[24] T.F. Yi, Y. Xie, Y.R. Zhu, R.S. Zhu, M.F. Ye, High rate micron-sized niobium-doped $LiMn_{1.5}Ni_{0.5}O_4$ as ultra high power positive-electrode material for lithium-ion batteries, J. Power Sources 211 (2012) 59–65.

[25] C. Locati, U. Lafont, L. Simonin, F. Ooms, E.M. Kelder, Mg-doped $LiNi_{0.5}Mn_{1.5}O_4$ spinel for cathode materials, J. Power Sources 174 (2007) 847–851.

[26] L. Zhou, D. Zhao, X. Lou, $LiNi_{0.5}Mn_{1.5}O_4$ Hollow Structures as High-Performance Cathodes for Lithium-Ion Batteries, Angew. Chem. 124 (2012) 243–245.

[27] C.W. Xiao, Y. Ding, J.T. Zhang, X.Q. Su, G.R. Li, X.P. Gao, P.W. Shen, $Li_{4-x}Na_xTi_5O_{12}$ with low operation potential as anode for lithium ion batteries, J. Power Sources 248 (2014) 323–329.

[28] B.L. Ellis, W.R.M. Makahnouk, W.N. Rowan-Weetaluktuk, D.H. Ryan, L.F. Nazar, Crystal Structure and Electrochemical Properties of A_2MPO_4F Fluorophosphates (A = Na, Li; M = Fe, Mn, Co, Ni), Chem. Mater. 22 (2009) 1059–1070.

[29] W. He, D. Yuan, J. Qian, X. Ai, H. Yang, Y. Cao, Enhanced high-rate capability and cycling stability of Na-stabilized layered $Li_{1.2}[Co_{0.13}Ni_{0.13}Mn_{0.54}]O_2$ cathode material, J. Mater. Chem. A 1 (2013) 11397–11403.

[30] T. Ohzuku, K. Ariyoshi, S. Takeda, Y. Sakai, Synthesis and characterization of 5 V insertion material of $Li[Fe_yMn_{2-y}]O_4$ for lithium-ion batteries, Electrochim. Acta 46 (2001) 2327–2336.

[31] G.B. Zhong, Y.Y. Wang, X.J. Zhao, Q.S. Wang, Y. Yu, C.H. Chen, Structural, electrochemical and thermal stability investigations on $LiNi_{0.5-x}Al_{2x}Mn_{1.5-x}O_4$ ($0 \leq 2x \leq 1.0$) as 5 V cathode materials, J. Power Sources 216 (2012) 368–375.

[32] S. Patoux, L. Daniel, C. Bourbon, H. Lignier, C. Pagano, F. Le Cras, S. Jouanneau, S. Martinet, High voltage spinel oxides for Li-ion batteries: From the material research to the application, J. Power Sources 189 (2009) 344–352.

[33] J.H. Kim, S.T. Myung, C.S. Yoon, S.G. Kang, Y.K. Sun, Comparative Study of $LiNi_{0.5}Mn_{1.5}O_{4-\delta}$ and $LiNi_{0.5}Mn_{1.5}O_4$ Cathodes Having Two Crystallographic Structures: Fd3m and $P4_332$, Chem. Mater. 16 (2004) 906–914.

[34] C.M. Julien, M. Massot, Lattice vibrations of materials for lithium rechargeable batteries I. Lithium manganese oxide spinel, Mater. Sci. Eng. B 97 (2003) 217–230.

[35] S.H. Oh, K.Y. Chung, S.H. Jeon, C.S. Kim, W.I. Cho, B.W. Cho, Structural and electrochemical investigations on the $LiNi_{0.5-x}Mn_{1.5-y}M_{x+y}O_4$ (M = Cr, Al, Zr) compound for 5 V cathode material, J. Alloy Compd. 469 (2009) 244–250.

[36] G.B. Zhong, Y.Y. Wang, Y.Q. Yu, C.H. Chen, Electrochemical investigations of the $LiNi_{0.45}M_{0.10}Mn_{1.45}O_4$ (M = Fe, Co, Cr) 5 V cathode materials for lithium ion batteries, J. Power Sources 205 (2012) 385–393.

[37] Y. Zhu, C. Wang, Novel CV for Phase Transformation Electrodes, J. Phys. Chem. C 115 (2010) 823–832.

[38] X. Wu, J. Zheng, Z. Gong, Y. Yang, Sol-gel synthesis and electrochemical properties of fluorophosphates $Na_2Fe_{1-x}Mn_xPO_4F/C$ (x = 0 0.1, 0.3, 0.7, 1) composite as cathode materials for lithium ion battery, J. Mater, Chem. 21 (2011) 18630–18637.

[39] S. Ivanova, E. Zhecheva, R. Stoyanova, D. Nihtianova, S. Wegner, P. Tzvetkova, S. Simova, High-Voltage $LiNi_{1/2}Mn_{3/2}O_4$ Spinel: Cationic Order and Particle Size Distribution, J. Phys. Chem. C 115 (2011) 25170–25182.